Title

Compare and contrast the reaction coordinate diagrams for chemical reactions and cytoskeletal force generators.

Journal

Molecular biology of the cell, 24(4)

ISSN

1059-1524

Author

Scholey, Jonathan M

Publication Date

2013-02-01

DOI

10.1091/mbc.e12-07-0545

Peer reviewed

Compare and contrast the reaction coordinate diagrams for chemical reactions and cytoskeletal force generators

Jonathan M. Scholey
Department of Molecular and Cell Biology, University of California, Davis, Davis, CA 95616

ABSTRACT **Reaction coordinate diagrams are used to relate the free energy changes that occur during the progress of chemical processes to the rate and equilibrium constants of the process. Here I briefly review the application of these diagrams to the thermodynamics and kinetics of the generation of force and motion by cytoskeletal motors and polymer ratchets as they mediate intracellular transport, organelle dynamics, cell locomotion, and cell division. To provide a familiar biochemical context for discussing these subcellular force generators, I first review the application of reaction coordinate diagrams to the mechanisms of simple chemical and enzyme-catalyzed reactions. My description of reaction coordinate diagrams of motors and polymer ratchets is simplified relative to the rigorous biophysical treatment found in many of the references that I use and cite, but I hope that the essay provides a valuable qualitative representation of the physical chemical parameters that underlie the generation of force and motility at molecular scales. In any case, I have found that this approach represents a useful interdisciplinary framework for understanding, researching, and teaching the basic molecular mechanisms by which motors contribute to fundamental cell biological processes.**

Monitoring Editor
Doug Kellogg
University of California, Santa Cruz

Received: Dec 3, 2012
Revised: Dec 13, 2012
Accepted: Dec 19, 2012

INTRODUCTION

Cytoskeletal motors and polymer ratchets play key roles in intracellular transport and dynamics, cytoplasmic organization, cell locomotion, and cell division, processes that lie at the heart of molecular cell biology (Bagshaw, 1993; Inoue and Salmon, 1995; Bray, 2001; Howard, 2001; Pollard and Borisy, 2003; Vale, 2003; Ishikawa and Marshall, 2011; Green *et al.*, 2012; McIntosh *et al.*, 2012). In addition, "moving parts" analogous to motors and polymer ratchets are used by a broad range of macromolecular machines to carry out their function (Alberts and Miake-Lye, 1992; Block *et al.*, 2007). Therefore to understand the fundamental problem of how molecules form living, moving, reproducing cells, we need to understand the underlying physical chemical principles by which motors and polymers generate force and motion.

DOI: 10.1091/mbc.E12-07-0545

Address correspondence to: Jonathan M. Scholey (jmscholey@ucdavis.edu).

Abbreviations used: AE, acyl enzyme intermediate; E, enzyme; G, Gibbs free energy; MT, microtubule; P, product; pf, protofilament; R, reactant; S, substrate; TI, tetrahedral intermediate; TS, transition state.

Here I briefly discuss the application of reaction coordinate (also known as energy landscape, potential energy) diagrams to chemical reactions, enzyme-catalyzed reactions, polymerizing–depolymerizing polymer ratchets, and cytoskeletal motors, which I believe provides a convenient format for relating cellular processes that depend on the generation of force and motion to simpler chemical and biochemical reactions. An essay that I enjoyed reading in these pages many years ago (Mitchison, 1992) motivated me to write this essay, with the caveat that the author of that essay is an expert researcher in the field that he discussed, whereas I have not done significant research on my topic, even though I follow it with interest, as it provides a foundation for my lab's research. My essay follows the theme of a series of lectures that I developed over several years of teaching about biological motors and macromolecular machines to biochemistry and cell biology students, drawing from material that is available in various textbooks and reviews, but that has not to my knowledge been presented together in a simplified, readily accessible form.

SIMPLE CHEMICAL REACTIONS

The basic features of a reaction coordinate diagram are conveniently illustrated with reference to a familiar S_N2 reaction as found in elementary organic chemistry texts (Figure 1; e.g.,

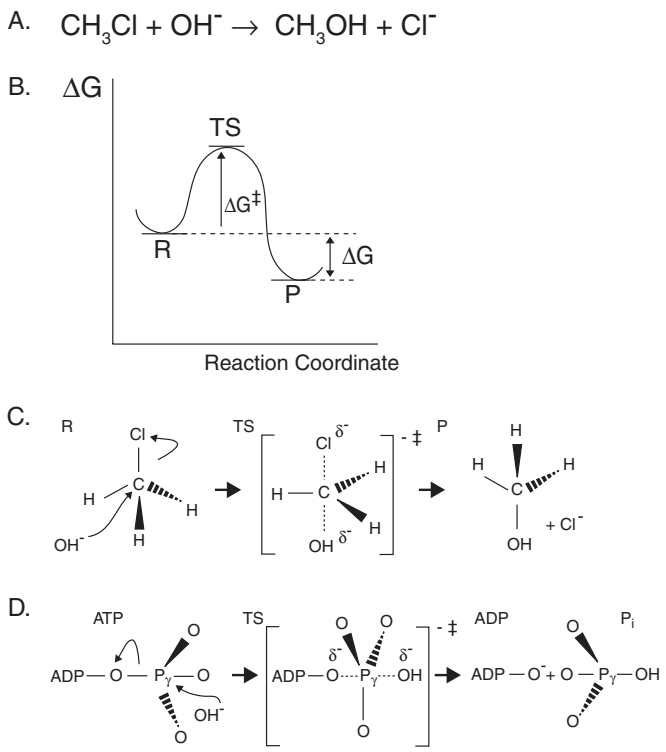

FIGURE 1: Reaction coordinate diagram for chemical reactions. (A) Equation for an S_N2 (substitution nucleophilic second order) reaction between a nucleophilic hydroxide ion and methyl chloride. (B) The reaction coordinate diagram for this reaction plots the changes in Gibbs free energy (ΔG) during the conversion of reactants (R) → TS → products (P). P has lower free energy than R, so this reaction is thermodynamically favorable, that is, it proceeds with the release of free energy: $\Delta G = -k_B T \ln K_{eq}$ is negative, so the equilibrium lies in the forward direction (k_B is Boltzmann's constant, T is temperature, and K_{eq} is the equilibrium constant). On the other hand, in order to react, R must acquire sufficient energy, the activation energy ($\Delta G^‡$), to form the high energy TS, which has equal probability of relaxing into R or P. $\Delta G^‡$ determines the reaction rate because the rate constant is given by $K = A \exp(-\Delta G^‡/k_B T)$, so a larger $\Delta G^‡$ means a smaller K and a slower reaction (the preexponential factor, A, relates to the collision frequency and orientation of R). This description is derived from kinetic theory (in which the thermal energy of a molecule [~2.5 kJ/mol at 25°C] of mass m and velocity v is related to its kinetic energy by $3/2\ k_B T = 1/2\ mv^2$) and the Maxwell–Boltzmann energy distribution of gas molecules at equilibrium, which describes the fraction of molecules with enough energy to react, gained through thermal collisions (Nelson, 2004, Chapter 3). (C) OH^- attacks the tetrahedral sp^3 C atom of CH_3Cl from the opposite side to the Cl leaving group, leading to inversion of configuration of the reaction center. The reaction proceeds via formation of a short-lived (10^{-12} s), high-energy transition state (TS) in which three H substituents are arranged trigonal planar to the now sp^2-hybridized carbon atom, whose remaining P orbital is used to form partial bonds to the attacking nucleophile and the leaving group. (D) The hydrolysis of ATP via in-line attack by OH^- to the γ-Pi proceeds by a similar mechanism.

Suggs, 2002, Chapter 8). In the example shown, the hydroxide nucleophile attacks the tetrahedral carbon atom of methyl chloride from the opposite side to the chloride leaving group, forming a short-lived, high-energy trigonal bipyramidal transition state (TS) that "relaxes" into the stable products, tetrahedral methanol and Cl^-.

The reaction coordinate diagram for this reaction plots the changes in Gibbs free energy (ΔG) during the conversion of reactants (R) to TS to products (P; Figure 1B). It can be seen that P is of lower free energy than R, so this reaction is thermodynamically favorable, that is, it proceeds in the direction of P with the release of free energy (ΔG is negative). On the other hand, in order to react, R must acquire sufficient energy, the activation energy ($\Delta G^‡$), to form the high-energy TS, which then has equal probability of relaxing into R or P. The magnitude of $\Delta G^‡$ determines how kinetically favorable is the reaction: the higher its value, the smaller is the rate constant, K, and the slower does the reaction proceed.

Note that reaction coordinate diagrams do not display all possible pathways for a specific reaction, only the most probable one. For example, the diagram for the hypothetical dissociation reaction AB → A + B plots ΔG against the increasing bond length A—B for only one, most probable bond angle but omits additional pathways that exist for a large number of less probable bond angles. In addition, it should be noted that a TS is different from a reaction intermediate, such as the carbo-cation that forms during an S_N1 (first order) reaction, where R reacts via a first TS to form the relatively stable carbo-cation intermediate (I), which then reacts via a second TS to form P.

The hydrolysis of ATP → ADP + Pi, which is more relevant to biological motors, occurs by a similar mechanism to the reaction of OH with methyl chloride, in that it involves the inline attack of γ-Pi by a nucleophilic OH or H_2O (Figure 1D; Bagshaw, 1993, p. 65). It proceeds to equilibrium with the release of large amounts of free energy ($\Delta G \approx -50$ kJ/mol or -10^{-19} J/molecule under cellular conditions). The released energy can in principle be used to do work, for example, by generating force and motion. However, the large $\Delta G^‡$ means that the uncatalyzed reaction proceeds to equilibrium very slowly (hours to days) in free solution and the released energy is dissipated as heat. Consequently, enzymes, that is, ATPases, such as the catalytic domains of cytoskeletal motors, are needed to make the reaction proceed at biologically useful rates (milliseconds to seconds) and to couple the released chemical free energy to mechanical work.

ENZYME-CATALYZED REACTIONS

The three-dimensional structure of each enzyme (be it a protein enzyme or a ribozyme) allows it to bind to a specific substrate (S) via multiple weak bonds and to undergo a conformational change, induced fit, in which mutual strain of E and S leads to formation of an E·TS complex in which TS has lower free energy ($\Delta G^‡$) than free TS. Thus, as reflected in the reaction coordinate diagram (Figure 2), the enzyme-active site provides an environment in which the stabilization of TS is paid for by the released "binding energy" (ΔG_B) as multiple weak bonds form. Here the binding energy "pays" for the lowering of the energy barrier, which enhances the rate constants for interconversion between S and P, with no effect on K_{eq}, but, as discussed later, a similar release of binding energy is used to generate pushing forces by polymer ratchets. Within the ES complex, substrate strain can also elevate the energy of the ground state, further facilitating TS formation. Thus enzymes massively enhance the rate at which equilibrium is attained; for example, catalase achieves a 10^{12}-fold enhancement of the rate of H_2O_2 decomposition (Nelson and Cox, 2000, Chapter 8; Kuriyan *et al.*, 2013, Chapter 16). Such stabilization of the TS by complementary fit between E and TS is a feature of the catalysis of ATP hydrolysis by the active site of the myosin-2 motor domain, for example. Here the inline attack of the tetrahedral γ-Pi of ATP by OH^- leads to formation of the trigonal bipyramidal γ-Pi of the TS, which then makes multiple, stabilizing

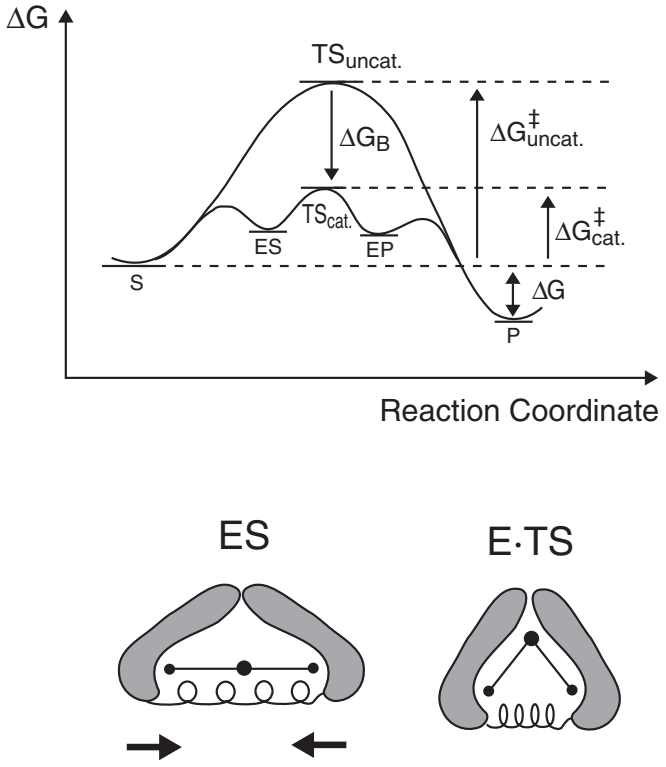

FIGURE 2: Reaction coordinate diagram of an idealized enzyme-catalyzed reaction. The reaction coordinate diagram shows that, to enhance the rate constants for crossing the activation energy barrier, S or P must obtain an amount of energy equal to that by which the activation energy is lowered. Much of this comes from the binding energy (ΔG_B) released due the formation of multiple weak bonds between the enzyme (E) and the TS, which, due to induced fit, are more complementary to one another than are E and S (shown in the lower schematic). In the reaction coordinate diagram, the activation energy for the catalyzed reaction, $\Delta G_{cat}^{\ddagger}$, is significantly lower than that of the uncatalyzed reaction, $\Delta G_{uncat}^{\ddagger}$, so the rate constant is correspondingly greater and the reaction is faster. However, the enzyme does not change the amount of free energy released or consumed (ΔG), and so K_{eq} is unchanged. For example, if the uncatalyzed forward and reverse rate constants for S ↔ P are $K_1 = 10^{-3}$ s^{-1} and $K_{-1} = 10^{-5}$ s^{-1}, respectively, then $Keq = K_1/K_{-1} = 100$. Catalysis 10^{14}-fold gives $K_1 = 10^{11}$ s^{-1} and $K_{-1} = 10^{9}$ s^{-1}; then K_{eq} remains 100.

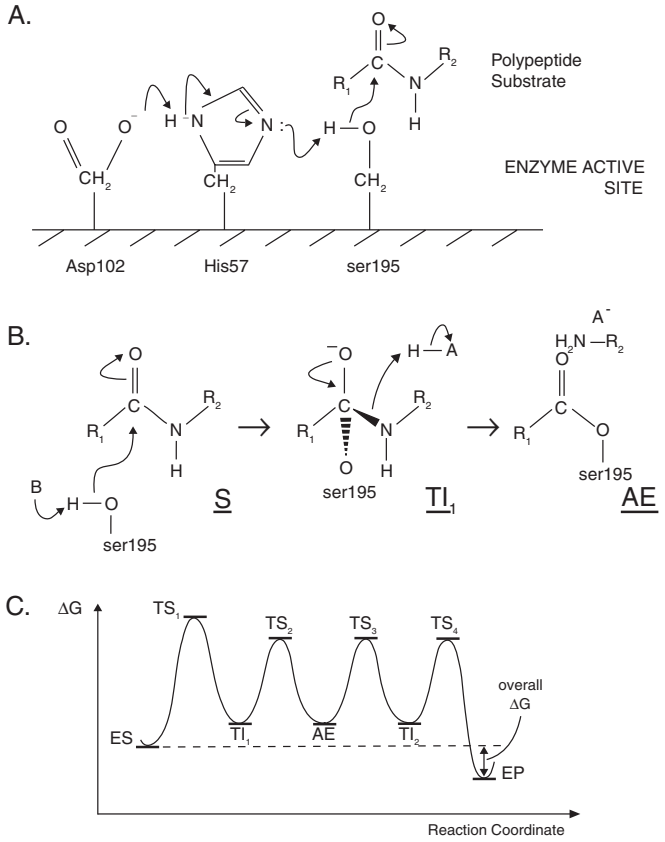

FIGURE 3: Real enzymes—serine proteases. (A) The catalytic triad of Ser-195, His-57, and Asp-102 appears in the enzyme-active site. The sp^2-hybridized trigonal planar carbon of the substrate's peptide bond is attacked by the nucleophilic hydroxyl group of Ser-195 in the active site. The adjacent His-57 is a general acid–base catalyst, which accepts H^+, converting Ser-195 to a better nucleophile, serine hydroxylate. Asp-102 forms a low-barrier H bond to His-57, enhancing its ability to withdraw H^+ from Ser-195. (B) Reaction showing formation of the acyl enzyme intermediate (AE), in which the serine hydroxylate acts as a nucleophile that attacks the sp^2 trigonal planar C of the peptide bond to be cleaved, forming a tetrahedral TS (not shown), which "relaxes" to form a relatively stable tetrahedral intermediate (TI_1), whose reactive C is now sp^3 hybridized. TI_1 accepts a proton from protonated His-57 (now acting as a general acid catalyst) to form TS_2, which relaxes to form the acyl enzyme (AE) intermediate, releasing the C-terminal segment of the substrate (R_2NH_2). In a second, similar reaction, H_2O acts as a nucleophile to attack the carbonyl C of AE, releasing the N-terminal portion of the polypeptide substrate via two additional TS and a second tetrahedral intermediate (TI_2; not shown). (C) The reaction coordinate diagram for such a real enzyme is obviously more complicated than the simplified case (Figure 2), containing four transition states ($TS_{1–4}$) and three intermediates ($TI_{1,2}$ and AE).

weak bonds to chemical groups brought into position by induced fit within the myosin-active site, thereby lowering the energy of the TS, leading to rate enhancement.

The situation is usually more complicated than the idealized case (Figure 2), as seen with reference to serine proteases (e.g., trypsin or chymotrypsin), which catalyze the hydrolysis of peptide bonds via mechanisms that are understood at atomic resolution (Figure 3; Williamson, 2012, Chapter 5). The enzyme's polypeptide chain folds up to bring the three amino acids of the catalytic triad into position to form a charge relay system that enhances nucleophilic attack of the substrate carbonyl group by Ser-195 (Figure 3A). This leads to the conversion of the trigonal carbonyl C via transition state (TS_1) to form a true tetrahedral intermediate (TI_1). TI_1 in turn abstracts a H^+ from protonated His-57 to form, via a second TS_2, the trigonal acyl-enzyme intermediate (AE) in which the NH_2-terminal segment of the substrate remains bound to Ser-195 and the COOH-terminal region is released (Figure 3B). A similar reaction involving two TS and a second TI_2 releases the amino-terminal end of the cleaved polypeptide chain. Thus the reaction coordinate diagram (Figure 3C) reflects a pathway that proceeds via four transition states, two tetrahedral intermediates and a covalently bonded acyl enzyme intermediate. In this reaction, the overall ΔG is negative and the formation of the first TS has the highest $\Delta G^{\ddagger}$ and thus represents the rate-limiting step.

POLYMER RATCHETS GENERATING "PUSHING" (COMPRESSIVE) FORCES

Given that all subcellular processes are based on (sometimes very elaborate) chemical reactions, it is perhaps not surprising that

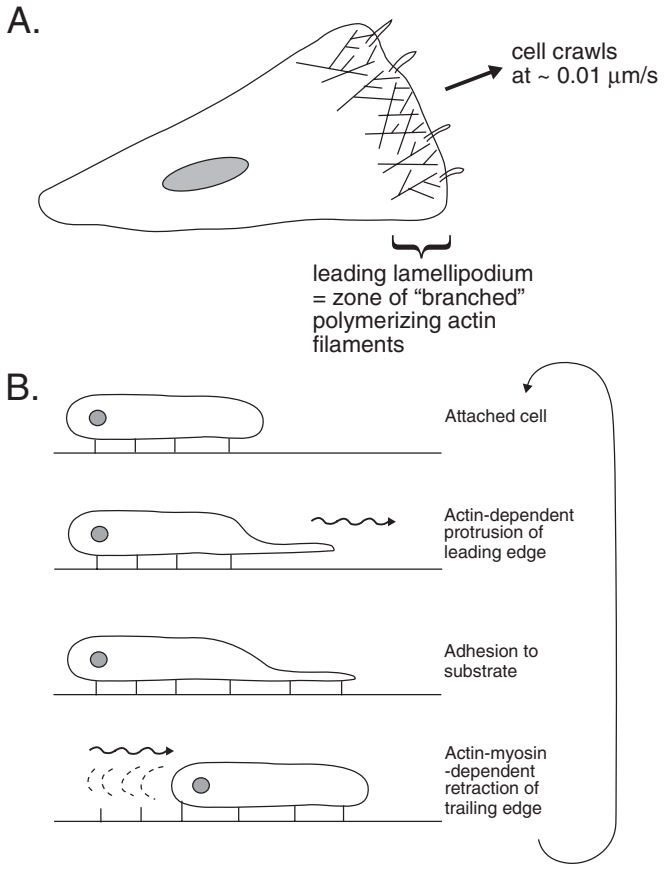

FIGURE 4: Schematic of a crawling cell. (A) Cartoon of fibroblast-type cell in tissue culture crawling over the substrate at ~0.01 μm/s using a branched dendritic network of actin filaments whose plus ends face the leading edge to polymerize and generate protrusive forces. The leading lamellipodium and a few filopodia are shown. The dendritic network involves binding of an Arp2/3 complex to the wall of each "mother" actin filament, where it nucleates polymerization of a daughter filament at an angle of 70°. The polymerization of the plus ends of these filaments can push against the cell membrane at the leading edge by a polymer ratchet mechanism (Pollard and Borisy, 2003). (B) The substrate-attached cell moves by using cycles of leading-edge protrusion coupled to exocytosis of new membrane, the establishment of new adhesions to the substrate, and actin-myosin–dependent retraction of the rear of the cell.

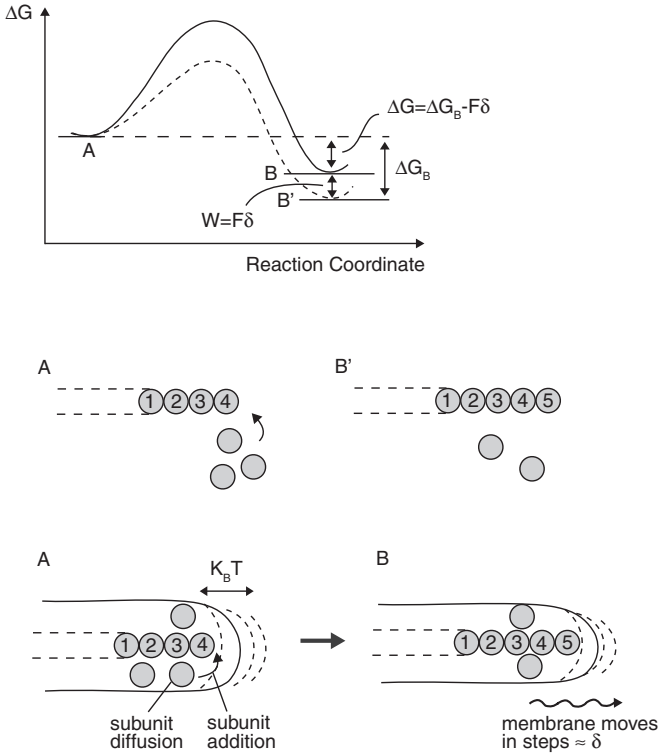

FIGURE 5: Reaction coordinate diagram for a polymer ratchet generating "pushing" (compressive) forces. The dashed line on the reaction coordinate diagram represents polymerization of a free actin filament; for example, the center shows a filament growing from an *n*-mer (with four subunits shown) to an (*n* + 1)-mer (with five subunits shown). The polymerization proceeds to the right with the release of free energy, the binding energy (ΔG_B) due to formation of new intersubunit bonds. The solid line shows the effect of the filament pushing against a load, for example, the leading membrane of a crawling cell (Figure 4). The membrane is shown undergoing random thermal motions under the influence of k_BT, such that when a gap is δ or greater, that is, the length by which the polymer grows due to addition of a single subunit, which for a two-strand actin filament is 5.5/2 = 2.75 nm, a new subunit can add onto the filament end. Thus the filament ratchets the membrane forward in a series of steps of distance δ. For each such step, work done on the membrane is given by W = force × distance = $F \times \delta$. This is paid for by the binding energy, so the overall free energy change for this pushing polymer ratchet is $\Delta G = \Delta G_B - F\delta$. For example, if $\Delta G_B = 10^{-20}$ J, F = 8 pN, and δ = 2.75 nm, then $F\delta \approx 3 \times 10^{-21}$ J, and overall $\Delta G = 7 \times 10^{-21}$ J.

biophysicists and modelers have been able to extend the foregoing analysis of relatively simple chemical and biochemical reactions (Figures 1–3) to more complex cell biological processes such as intracellular transport, cell locomotion, and cell division (Figures 4–7). In the latter cases, to be discussed later, the molecular and quantitative details are generally less well understood than for the examples discussed previously; for example, the intermediates and transition states are not well defined, and thus the free energy profiles linking the initial and final states represent only intuitively appealing approximations of the true pathways.

One interesting example is the polymer ratchet mechanism for leading-edge protrusion in cells that move by crawling over a surface. Most cell biology texts depict a crawling cell as undergoing cycles of leading-edge protrusion mediated by a zone of polymerizing actin, adhesion to the substratum, and actin-myosin–mediated trailing-edge retraction (Figure 4). Leading-edge protrusion has been extensively researched and is now understood to involve branched dendritic arrays of F-actin filaments in which actin polymer ratchets exert pushing forces that cause the cell membrane to protrude (Pollard and Borisy, 2003; Figure 5).

A simple way in which polymerizing actin filaments (or microtubules [MTs]) are proposed to generate pushing forces is via a thermal or Brownian ratchet mechanism (Feynman *et al.*, 1963; Theriot, 2000; Howard, 2001; Mogilner and Oster, 2003; Phillips *et al.*, 2009). In this model, the object being moved, for example, the cell membrane, undergoes random thermal motions at the growing plus end of the polymerizing filament. In the absence of the filament the object would simply undergo random thermal motion, that is, diffusion. However, the presence of the polymerizing filament serves to "rectify" these random motions, making movement directional. This is because, when such random motion produces a gap of sufficient size between the filament tip and the membrane, a subunit can

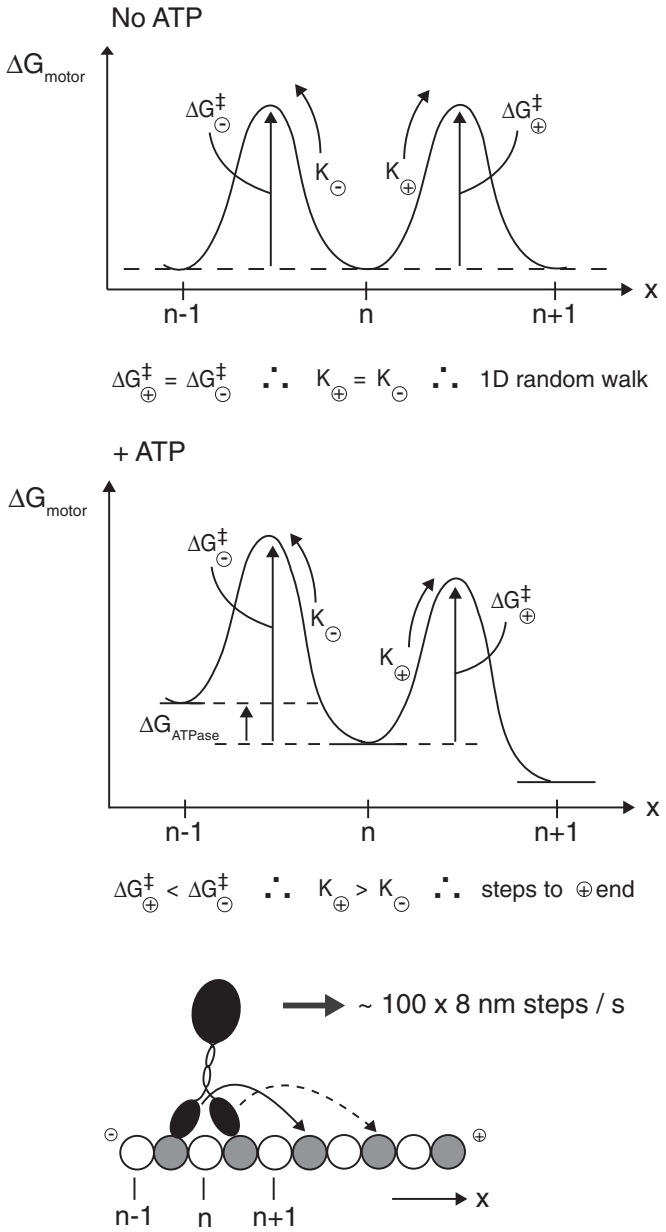

FIGURE 6: Reaction coordinate diagram for a motor stepping along a polymer track whose plus (⊕) end is oriented to the right. The reaction coordinate diagrams show the free energy change for a motor moving a distance *X* along a polymer track in the absence (top) and presence (center) of ATP fuel, which serves to bias random thermal motion in favor of vectorial movement. The cartoon (bottom) shows a kinesin motor stepping along a microtubule protofilament made of αβ-tubulin dimers with the β-tubulin facing the plus end of the microtubule. The motor starts at subunit *n* and can move δ = 8 nm in either the forward direction to subunit *n* + 1 or backward to subunit *n* – 1 in each discrete time step. In the absence of ATP (top) the activation energy for moving forward ($\Delta G_+^{\ddagger}$) is equal to the activation energy for moving backward ($\Delta G_-^{\ddagger}$), and hence the rate constants, that is, the probabilities of stepping forward or backward, are equal, and the motor diffuses randomly along the MT track executing a one-dimensional random walk where mean square displacement is given by $\langle X^2 \rangle = 2Dt$, where *D* is the diffusion coefficient and *t* is elapsed time. This equation describes a Gaussian probability distribution of the motor's position at a given time. ATP binding and hydrolysis by the kinesin motor domain releases free energy, which biases the random walk by tilting the energy landscape to the right, that is, toward the plus end of the MT (center). Now the activation energy ($\Delta G_+^{\ddagger}$) for stepping forward from subunit *n* to *n* + 1 is less than the activation energy for backstepping ($\Delta G_-^{\ddagger}$), and because $K = A \exp -\Delta G^{\ddagger}/k_BT$, the rate constant ($K_+$) for stepping forward is greater than that for stepping backward (K_-). Hence the random walk driven by thermal energy is "rectified" or biased in favor of forward steps, and the kinesin motor steps persistently to the plus end of the MT, rendering backstepping unlikely. Here the motor's mean-square displacement combines random diffusion with net drift, $\langle X^2 \rangle = 2Dt + Vt^2$, and so now the mean of the spreading Gaussian moves persistently toward the MT plus end with drift velocity, *V*. Under the low–Reynolds number conditions that apply here, $F = \mu V$, where *F* is force generated by the motor, μ is the viscous drag coefficient, and *V* is the motor's velocity.

diffuse into the gap and add onto the end of the filament. The addition of one subunit moves the membrane a net distance δ = 2.75 nm, that is, the length increase produced by addition of one G-actin subunit to an actin filament, and thus the addition of multiple subunits causes the membrane to ratchet forward in increments of δ.

To move the membrane directionally in this way, work must be done, which requires a supply of energy. As seen in the reaction coordinate diagram in Figure 5, the addition of a subunit to the end of the filament produces new subunit–subunit bonds, releasing free energy (ΔG_B), which is analogous to the binding energy between an enzyme and its substrate discussed earlier. Whereas the binding energy released by enzyme–substrate interactions is used to generate mutual strain of the enzyme and substrate and to pay for lowering the activation energy and thereby stabilizing the transition state, the binding energy released upon actin polymerization can be used to generate pushing forces on an object, where work done = force applied to object (*F*) times the distance the object is moved (δ). Thus, whereas the polymerization of a free actin filament yields free energy equal to ΔG_B per subunit added, the overall free energy change for an equivalent filament pushing against a load is given by $\Delta G = \Delta G_B - F\delta$ (Figure 5). It has been shown that the amount of free energy liberated by addition of an actin subunit to a filament is the product of the equilibrium (maximal) force (F_{eq}) and δ, so that $F_{eq}\delta = k_BT \ln(C_1/C_c)$, where C_1 is the concentration of polymerization-competent actin subunits and C_c is the critical concentration (Howard, 2001, Chapter 10). Thus for a leading edge in which C_1 = 30 μM and C_c = 0.1 μM, F_{eq} = 8 pN and $\Delta G_B \approx 10^{-20}$ J/subunit, which is less than the energy released by the hydrolysis of a molecule of ATP (10^{-19} J) but is greater than k_BT (4.1×10^{-21} J/molecule) and is believed to be capable of generating the piconewton-scale forces required to protrude the leading-edge membrane at the rates observed.

CYTOSKELETAL MOTOR PROTEINS

Whereas pushing polymer ratchets use binding energy to "rectify" random thermal motions and generate force and directional movement, cytoskeletal motors use the ~10^{-19} J/molecule free energy released from ATP hydrolysis to accomplish the same thing (see Phillips *et al.*, 2009, Chapter 16, for a very clear, rigorous discussion). For example, a kinesin motor that hydrolyzes one ATP per step and steps along a MT with δ = 8 nm and K_{cat} = 75 ATP/s can use the energy released to move at an "unloaded" velocity given by $V = 8 \times 75 = 600$ nm/s. However, above a certain threshold opposing force, the motor will slow down as the force increases, yielding a characteristic "force–velocity curve." The motor stops or stalls when it devotes all of the available energy of ATP hydrolysis to generate its maximal hypothetical force, $F_{stall} = \Delta G_{ATPase}/\delta = 10$ pN. The stall force of kinesin-1 has been estimated experimentally to be 6 pN, suggesting that some of the energy released by ATP hydrolysis is

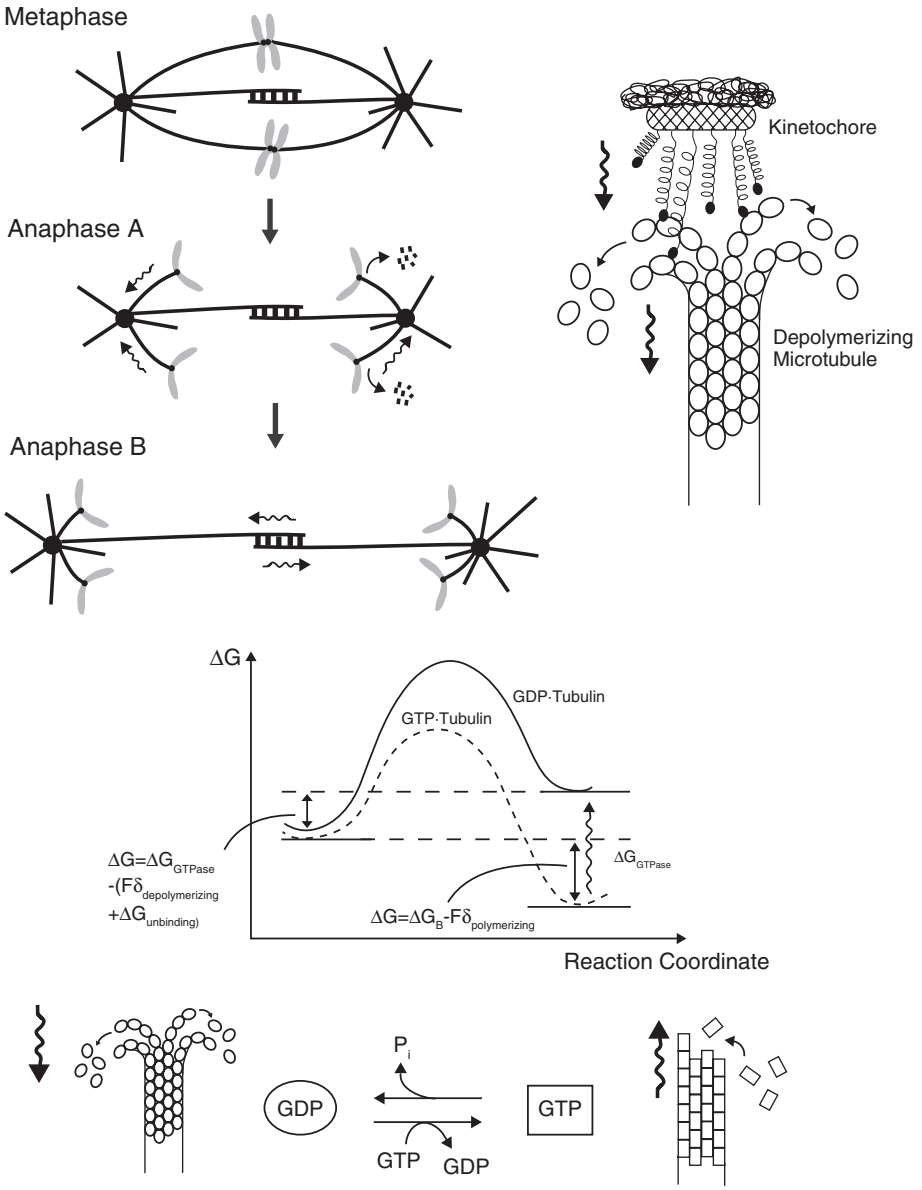

FIGURE 7: A polymer ratchet generating "pulling" (tensile) forces. During mitosis, chromosomes are separated by two processes—anaphase A, during which chromosomes are pulled toward the spindle poles by depolymerizing MTs, and anaphase B, during which the spindle poles are moved apart, pulling the chromosomes along and further separating them (top left). In the "Pac-Man" component of anaphase A, the depolymerizing MT "pulls" on the kinetochore, but how a depolymerizing MT exerts a pulling force and maintains kinetochore attachment is an area of active investigation. In one model, the kinetochore attaches to a depolymerizing MT via multiple "fibrils," each of which dynamically binds and releases the end of the shortening MT as the ensemble of fibrils maintains overall attachment (top right). The hydrolysis of GTP by tubulin within the MT polymer lattice releases free energy, which strains the polymer lattice, driving depolymerization, which is accompanied by the fraying apart and curling of the MT protofilaments (pfs). This pf curling pulls the kinetochore poleward. On the corresponding reaction coordinate diagram (center) the dashed curve shows the dynamics of GTP tubulin, which tends to polymerize as multiple weak bonds form between the complementary surfaces of the tubulin subunits. The equilibrium for this reaction lies in the forward direction, and as the MT grows from an *n*-mer (left) to an (*n* + 1)-mer (right), binding energy (ΔG_B) is released, but if the polymer pushes on a chromosome, moving it a distance δ, the overall free energy change is reduced to $\Delta G = \Delta G_B - F\delta$ (as for actin in Figure 5). The solid curve shows the free energy change associated with depolymerizing GDP-tubulin MTs. The hydrolysis of GTP by tubulin within the MT polymer lattice releases free energy ΔG_{GTPase}, which strains the lattice, elevating the free energy, so that now the free energy of the (*n* + 1)-mer is greater than that of the *n*-mer and depolymerization is favored. The free energy released by GTP hydrolysis is stored as elastic energy within the polymer and can be released during depolymerization and used to pay for the "unbinding" of tubulin subunits as they depolymerize and also to exert pulling (tensile) force on a load, for example, a chromosome, moving it a distance δ toward the spindle pole, so that work done is given by $W = F\delta$. Thus the overall free energy change as the MT depolymerizes by one subunit and pulls the chromosome poleward is $\Delta G = \Delta G_{GTPase} - (F\delta + \Delta G_{unbinding})$.

dissipated as friction. Under the low–Reynolds number conditions that govern motion at this scale (Bray, 2001, Chapter 1), the movement of a 1-μm-diameter transport vesicle at velocity $V = 6 \times 10^{-7}$ m/s through cytoplasm of viscous drag coefficient $\mu = 2 \times 10^{-6}$ N s/m requires the continual application of a force $F = \mu V \approx 1$ pN, which is significantly less than the stall force for a single motor.

Figure 6 depicts reaction coordinate diagrams for such a kinesin motor moving at its unloaded velocity along a MT. The motor is initially positioned at subunit *n* on a MT protofilament (pf) in the absence (top) or presence (middle) of ATP. In the absence of ATP, the motor can step a distance δ either to the right (to subunit *n* + 1) or the left (to subunit *n* – 1) with equal probability under the influence of random thermal energy. This is reflected in the corresponding reaction coordinate diagram, in which the forward and reverse activation energies $\Delta G^{\ddagger}$, and therefore the corresponding rate constants, are equal. Thus if the motor is constrained to a single pf, it will execute a one-dimensional random walk, that is, diffuse randomly back and forth along the pf. The free energy released by ATP hydrolysis is used to effectively "tilt the energy landscape" so that the activation energy for stepping toward the plus end of the MT pf is much less than that for stepping backward, meaning that the rate constant for stepping forward from subunit *n* to subunit *n* + 1 is much greater than the probability of stepping backward from *n* to *n* – 1. Now the motor steps persistently forward toward the plus end of the MT, undergoing diffusion with drift in accordance with the low–Reynolds number regime that applies at molecular scales. An opposing force of increasing magnitude will counteract the tilting of the energy landscape resulting from ATP hydrolysis, "untilting" it by an amount proportional to the magnitude of the force, so that the motor slows down and eventually stalls, accounting for its force–velocity curve.

POLYMER RATCHETS GENERATING "PULLING" (TENSILE) FORCES

The use of depolymerizing polymer ratchets to generate pulling forces has been

extensively discussed, especially with reference to kinetochore MTs that shorten to pull chromosomes toward the mitotic spindle poles via a kinetochore-based "Pac-Man" mechanism (Inoue and Salmon, 1995; McIntosh *et al*., 2008). I have not found any published reaction coordinate diagrams for such a pulling MT polymer ratchet, but perhaps the one I put together for teaching purposes shown in Figure 7, or something similar, represents a reasonable starting point.

In this case, GTP-tubulin subunits in the "relaxed" conformation tend to polymerize via a reaction pathway that releases binding energy (ΔG_B), that is, similar to the case for actin polymerization discussed earlier (Figure 4). In the spindle, such a growing MT could serve as pushing polymer ratchet that would apply a "polar ejection" force, *F*, to push chromosome arms and possibly kinetochores a distance δ per subunit added in a direction away from the spindle poles, so again the overall free energy drop is $\Delta G = \Delta G_B - F\delta$. For this reaction to proceed in reverse, converting the MT to a "pulling" polymer ratchet requires a supply of free energy, which comes from the hydrolysis of bound GTP by the β-tubulin subunits within the polymer lattice ($\Delta G_{GTPase} \approx 10^{-19}$ J/molecule; Figure 7). This converts tubulin to a strained, "tense" conformation in which an (*n* + 1)-mer is less stable and has a higher Gibbs free energy than a corresponding *n*-mer. Consequently the MT now has a tendency to depolymerize with release of free energy that can generate tensile force, *F*, on a chromosome to pull it a distance δ per subunit lost (Figure 7). Structurally at the kinetochore, the pfs of the plus ends of depolymerizing MTs tend to fray and curve downward toward their opposite minus ends located at the spindle poles, and it is proposed that ensembles of "kinetochore fibrils" that each dynamically attach to and release from the curving pfs are responsible for maintaining the attachment of the kinetochore, and hence the chromosome, to the end of the depolymerizing MT (McIntosh *et al*., 2008). It is estimated that this mechanism can generate a force of tens of piconewtons per MT, far greater than the 1-pN force required to move the chromosome at rates observed against viscous drag, based on similar arguments to those discussed earlier for the kinesin motor. By comparison, the maximal force that an anaphase spindle is believed to exert on a chromosome ($F_{stall} \approx 0.7$ nN) corresponds to ~50 pN/kMT for a kinetochore fiber consisting of 15 kMTs pulling the chromosome to the pole during anaphase A (Nicklas, 1983).

SUMMARY

In accord with reductionist principles (Crick, 1988), reaction coordinate diagrams provide a general picture of the physical chemical principles by which macromolecular machines contribute to the organization and function of living cells because they display in an idealized and simplified manner the thermodynamics and kinetics of enzymes, polymer ratchets, and motors. My description of reaction coordinate diagrams obviously oversimplifies the true mechanism compared with the more rigorous biophysical treatments that can be found in many of the cited references. On the other hand, the latter presentations rarely, if ever, seem to discuss how these diagrams (Figures 5–7) also apply to much simpler, more familiar chemical and biochemical reaction mechanisms (Figures 1–3). Conversely, the chemistry and biochemistry texts that I have used in class do not discuss the reaction coordinate diagrams of cytoskeletal motors and polymer ratchets. Even though my laboratory has not done significant work in the area of the biophysical mechanisms of cytoskeletal force generators, I have found these diagrams to be valuable both as an interdisciplinary tool for teaching biochemistry and cell biology majors and as a mechanistic foundation for our research on mitosis, intraflagellar transport/cilium biogenesis, and motor protein function. One significant advantage is their generality; that is, just as there exist a vast number of different organic reactions that conform to the reaction coordinate diagram for an S_N2 reaction (Figure 1), it seems reasonable to believe that cytoskeletal motors, including kinesins, dyneins, and myosins, as well as other translocating motors, such as helicases moving along DNA, all conform to a reaction coordinate diagram of the type shown in Figure 6. On the other hand, such a general picture is obviously limited, and for each specific case it is necessary to dig deep into the detailed nuts and bolts to develop a precise quantitative and atomic resolution picture of its particular mechanism (Vale and Milligan, 2000).

ACKNOWLEDGMENTS

I thank the students and colleagues who provided constructive feedback on this material over the years and Gul Civelekoglu-Scholey for comments on the manuscript. Generous support for my work has been provided by National Institutes of Health Grants GM50718 on Intraflagellar Transport Motors and Ciliogenesis in *C. elegans* Neurons and GM55507 on Dynamics of Mitosis in *Drosophila* Embryos: Mechanism of Anaphase B.

REFERENCES

Alberts B, Miake-Lye R (1992). Unscrambling the puzzle of biological machines: the importance of the details. Cell 68, 415–420.
Bagshaw CR (1993). Muscle Contraction, 2nd ed., London: Chapman and Hall.
Block SM, Larson MH, Greenleaf WJ, Herbert KM, Guydosh NR, Anthony PC (2007). Molecule by molecule, the physics and chemistry of life: SMB 2007. Nat Chem Biol 3, 193–197.
Bray D (2001). Cell Movements: From Molecules to Motility, New York: Garland Publishing.
Crick FHC (1988). What Mad Pursuit: A Personal View of Scientific Discovery, New York: Basic Books.
Feynman RP, Leighton RB, Sands M (1963). The Feynman Lectures on Physics, Reading, MA: Addison-Wesley.
Green RA, Paluch E, Oegema K (2012). Cytokinesis in animal cells. Annu Rev Cell Dev Biol 28, 29–58.
Howard J (2001). Mechanics of Motor Proteins and the Cytoskeleton, Sunderland, MA: Sinauer.
Inoue S, Salmon ED (1995). Force generation by microtubule assembly/disassembly in mitosis and related movements. Mol Biol Cell 6, 1619–1640.
Ishikawa H, Marshall WF (2011). Ciliogenesis: building the cell's antenna. Nat Rev Mol Cell Biol 12, 222–234.
Kuriyan J, Konforti B, Wemmer D (2013). The Molecules of Life, New York: Garland Science.
McIntosh JR, Grishchuk EL, Morphew MK, Efremov AK, Zhudenkov K, Volkov VA, Cheeseman IM, Desai A, Mastronarde DN, Ataullakhanov FI (2008). Fibrils connect microtubule tips with kinetochores: a mechanism to couple tubulin dynamics to chromosome motion. Cell 135, 322–333.
McIntosh JR, Molodtsov MI, Ataullakhanov FI (2012). Biophysics of mitosis. Q Rev Biophys 45, 147–207.
Mitchison TJ (1992). Compare and contrast actin filaments and microtubules. Mol Biol Cell 3, 1309–1315.
Mogilner A, Oster G (2003). Polymer motors: pushing out the front and pulling up the back. Curr Biol 13, R721–R733.
Nelson DL, Cox MM (2000). Lehninger Principles of Biochemistry, New York: Worth Publishers.
Nelson P (2004). Biological Physics, San Francisco: WH Freeman.
Nicklas RB (1983). Measurements of the force produced by the mitotic spindle in anaphase. J Cell Biol 97, 542–548.
Phillips R, Kondev J, Theriot J (2009). Physical Biology of the Cell, New York: Garland Science.
Pollard TD, Borisy GG (2003). Cellular motility driven by assembly and disassembly of actin filaments. Cell 112, 453–465.
Suggs JW (2002). Organic Chemistry, Hauppage, NY: Barron's.
Theriot JA (2000). The polymerization motor. Traffic 1, 19–28.
Vale RD (2003). The molecular motor toolbox for intracellular transport. Cell 112, 467–480.
Vale RD, Milligan RA (2000). The way things move: looking under the hood of molecular motor proteins. Science 288, 88–95.
Williamson M (2012). How Proteins Work, New York: Garland Science.